Published in final edited form as:
Mol Imaging Biol. 2011 December ; 13(6): 1163–1172. doi:10.1007/s11307-010-0424-8.

Trafficking of a Dual-Modality Magnetic Resonance and Fluorescence Imaging Superparamagnetic Iron Oxide-Based Nanoprobe to Lymph Nodes

Ambika Bumb[1], **Celeste A. S. Regino**[2], **Jackson G. Egen**[3], **Marcelino Bernardo**[2,4], **Peter J. Dobson**[5], **Ronald N. Germain**[3], **Peter L. Choyke**[2], and **Martin W. Brechbiel**[1]

[1] Radiation Oncology Branch, National Cancer Institute, National Institutes of Health, Bethesda, MD 20892, USA

[2] Molecular Imaging Program, National Cancer Institute, National Institutes of Health, Bethesda, MD 20892, USA

[3] Laboratory of Immunology, National Institute of Allergy and Infectious Diseases, National Institutes of Health, Bethesda, MD 20892, USA

[4] SAIC-Frederick Inc., NCI-Frederick, Frederick, MD 21702, USA

[5] Oxford University Begbroke Science Park, Oxon OX5 1PF, UK

Abstract

Purpose—To develop and characterize the trafficking of a dual-modal agent that identifies primary draining or sentinel lymph node (LN).

Procedure—Herein, a dual-reporting silica-coated iron oxide nanoparticle (SCION) is developed. Nude mice were imaged by magnetic resonance (MR) and optical imaging and axillary LNs were harvested for histological analysis. Trafficking through lymphatics was observed with intravital and *ex vivo* confocal microscopy of popliteal LNs in B6-albino, CD11c-EYFP, and *lys*-EGFP transgenic mice.

Results—*In vivo*, SCION allows visualization of LNs. The particle's size and surface functionality play a role in its passive migration from the intradermal injection site and its minimal uptake by CD11c+ dendritic cells and CD169+ and *lys*+ macrophages.

Conclusions—After injection, SCION passively migrates to LNs without macrophage uptake and then can be used to image LN(s) by MRI and fluorescence. Thus, SCION can potentially be developed for use in sentinel node resections or for intralymphatic drug delivery.

Keywords

nanoparticle; molecular imaging; MRI; optical imaging; lymph node; superparamagnetic iron oxide

INTRODUCTION

With its small channels that are not directly accessible, the lymphatic system is complex and difficult to examine *in vivo*. Multiple afferent "collector" vessels from proximal tissue enter

*Address for Correspondence: Martin Brechbiel, PhD, Radioimmune & Inorganic Chemistry Section, Radiation Oncology Branch, NCI, NIH, Building 10 Room 1B53, 10 Center Drive, Bethesda, MD 20892. Tel: +1 301-496-0591. Fax: +1 301-402-1923., martinwb@mail.nih.gov.

the sinus of the lymph node (LN) outer cortex where innate immunity, a primary defense, can take place. The lymph fluid then drains from the hilum of the LN out the efferent vessel and on through the lymphatic network. Understanding and visualizing lymphatic flow is important as it can be altered during disease states and because of its use as a route for vaccine delivery. Evaluating the primary draining or sentinel lymph nodes (SLNs) from a tumor basin is crucial information on which both the prognosis and therapy of carcinomas depend, e.g. it is a major criterion for determining the need for adjuvant chemotherapy in breast cancer patients. They are the most likely site to potentially to contain metastatic cells [1] and their status accurately reflects that of the more distant axillary lymph nodes, wherein a negative biopsy indicates a >95% chance that the remaining nodes are also cancer free [2]. Currently, two agents are used to identify sentinel nodes during breast surgery [3–5]. After peritumoral or periareolar injection of blue dye isosulfan and/or a radiolabeled macromolecule such as ^{99m}Tc-albumin or sulfur colloid, SLNs are detected by a handheld γ-ray counter and/or by their blue color upon deeper dissection of tissue. They are then excised for histology and immunohistochemistry. External detection of radioactivity within a node can be difficult with the handheld gamma counter because it may be hard to separate the node from the injection site. Also, radioscintigraphy results in radiation exposure for the surgery staff and patient. The blue dye can only be seen by direct vision when the surgeon exposes the sentinel node and often leaves a blue stain on the overlying skin that can persist for months after surgery. Thus, an alternative and non-invasive approach that assists in the accurate identification of lymph node metastases without radiation would be ideal for patients and clinicians.

Radionuclide, optical, as well as, magnetic resonance imaging (MRI) methods are now available both pre-clinically and clinically for lymphatic imaging [6,7]. Ultrasmall superparamagnetic iron oxide particles (USPIOs) are a class of nanoprobes that provide strong T_2 contrast for MRI. They have been used for magnetic resonance lymphangiography (MRL) when administered intravenously, however not by peritumoral injection for sentinel node detection. MRI does not involve radiation exposure, offers good spatial resolution, and non-invasively provides functional and anotomical information using innate tissue contrast. MRL with a contrast agent allows for LN internal structure to be visualized rather than relying on current methods of measuring nodal size as the primary yardstick for differentiating benign from malignant lymph nodes. Though MRI is useful for pre-operative planning, it is not practical for intraoperative use during sugical ressection of SLNs. A potential solution is fluorescence imaging using portable equipment compatible with the operating room environment. In addition to being more sensitive than MRI and not requiring radiation exposure, fluorescence imaging has high temporal and spatial resolution, and permits real-time visualization below the skin surface. Optical agents with near infrared (NIR) emissions (~700–900 nm) can be visualized from tissue depths of several centimeters, albeit with considerable diffusion, as the absorption coefficient of tissue is considerably smaller in the NIR region [8,9]. Additionally, NIR fluorophores, such as Cy5.5, minimize signal contamination from autofluorescence arising from intrinsic biomolecules typically occurring in the visible light spectrum, 350–700 nm [10,11]. NIR fluorescence imaging systems that simultaneously display color video and NIR images have been developed for real-time surgical applications [12,13]. Sentinel node imaging with a dual-modality MR/NIR agent would allow for detailed anatomical information by MRI (pre-operatively) and real-time guidance for the surgeon by fluorescence imaging (intraoperatively).

Herein, we describe a novel 18–20 nm dual-imagable silica-coated iron oxide nanoparticle (SCION) and its application for SLN imaging. We further study the transport of the particle from its injection site to SLNs and its subsequent localization within the node.

MATERIALS AND METHODS

SCION Synthesis and Characterization

Two lots of SCION particles, SCION(Cy5.5) and SCION(AlexaFluor555) were synthesized using the method described in Bumb et al [14,15]: one with fluorophore Cy5.5 (excitation/emission maxima ~675/694 nm) and the second with AlexaFluor555 (excitation/emission maxima ~555/565 nm). The two fluorophores were purchased with a *N*-hydroxysuccinimide (NHS) ester group: NIR cyanine Cy5.5 (GE Healthcare) and AlexaFluor555(Invitrogen). The synthesis is summarized in Fig. 1.

Iron content was analyzed in duplicate by inductively coupled plasma optical emission spectrometry (ICP-OES, Colombia Analytical Services, Tucson, Arizona). Using a Malvern Zetasizer Nano ZS, the hydrodynamic diameter by number distribution and zeta potential of the SCION particles were evaluated (n=5). All sample readings fell within detection limits. Adjustments in pH were made with solutions of 0.1M potassium hydroxide and hydrochloric acid.

The relaxivity of SCION particles was compared to that of the T_1 agent Gd-DTPA (Magnevist, Bayer Healthcare Pharmaceuticals) and T_2 agent Feridex (Bayer Healthcare Pharmaceuticals), a larger (80–150 nm) dextran-coated iron oxide particle. While Gd-DTPA solutions (0–2.0 mM Gd) were diluted in water, SCION and Feridex preparations (0–1.0 mM Fe) were in 0.25% agarose water gels to ensure even dispersion and to prevent particles from migrating to tube periphery while in the MR magnet. Relaxivity measurements on duplicate samples were obtained at room temperature (~22°C) using a 3T clinical scanner (Signa Excite, General Electric Medical System, Waukesha, WI, USA) equipped with a rectangular single loop receiver coil (84 × 126 × 6 mm). For T_1 calculations, images of the solutions using a 2D-spin echo (2D-SE) sequence were acquired with repetition times (TR) of 100, 350, 750, 1250, 2500 and 5000 ms at echo time (TE) of ~11 ms. For T_2 analysis, the sequence was an 8-echo spin-echo with TR = 5000 ms and TE ≈ 9 ms. T_1 and T_2 maps were calculated using ImageJ MRI Analysis plug-in (www.rsb.info.nih.gov/ij/plugins/mri-analysis.html).

In Vivo Sentinel LN Imaging Studies

Female athymic (*nu/nu*) mice were purchased from Charles River Laboratories at 4–6 weeks of age and housed in a specific pathogen-free American Association for Laboratory Animal Care approved facility. Animals were used between 6 and 8 weeks of age and experiments were approved by the National Cancer Institute's Animal Care and Use Committee. MR images were obtained using a 3T clinical scanner (Achieva Intera, Philips Healthcare, Best, Netherlands) equipped with a mouse-sized solenoidal coil with an inner diameter of 40 mm and a coil length of 40 mm (Philips Research, Hamburg, Germany). With fat suppression by spectral pre-saturation attenuated inversion recovery (SPAIR), respiratory triggered T_2-weighted multi-slice spin-echo images (repetition time of 4000 ms, echo time of 30 ms, 90° flip angle, voxel size of 0.15 × 0.15 × 0.6 mm, resolution of 6.6 pixels per mm) were obtained prior to injection of the agent (t = 0 hr) and post-injection at 24 hr. Mice were anesthetized using gas mixtures of 1.5–2.5% isoflurane in O_2 to maintain a respiration rate of ~30 bpm during the entire MRI scan. A volume of 10 μL of a 40 mM [Fe] of SCION(Cy5.5) solution in saline was intradermally injected into the left footpad of each mouse, with the right side as a control. Previous studies have shown that the primary draining LNs from this injection site are the axillary and lateral thoracic LNs [16]. Approximately 24 hr post-injection, the mice were scanned a second time, and after acquisition of MRI data, optical imaging of the same mice was performed using a Maestro CRi spectroscopic optical camera to generate matched sets. The axillary and lateral thoracic

lymph nodes were then excised and fixed in formalin. The fixed axillary LN tissue was sent to Mass Histology (Worcester, Massachusetts) where histologic slides were prepared and analyzed by hematoxylin and eosin stain and Prussian blue iron stain on a nuclear fast red background.

Trafficking through Lymphatics

B6(Cg)-*Tyr*$^{c\text{-}2J}$/J C57BL/6 mice, or B6-albino mice, were purchased from the Jackson Laboratory (Bar Harbor, Maine). These different strains of mice were used to illuminate and stain for cell markers of particular cell types that play a role in transport to or in the LN. CD11c-EYFP [17] mice were originally a gift from Michel Nussenzweig (Rockefeller University, New York) and *lys*-EGFP [18] from Thomas Graf (Center for Genomic Regulation, Spain). All mice were maintained in the NIH animal facilities and all procedures performed were approved by the National Institute of Allergy and Infectious Diseases's Animal Care and Use Committee.

The apparatus setup for intravital imaging through the lymphatics required using the hind legs and exposing the lympatic vessel leading from the hind foot to the popliteal LN. Thus injections were performed in the hind foot pad for this set of studies. It also allowed for demonstration of agent draining to LNs from a different injection site. Solutions of 30 mM [Fe] of SCION(AlexaFluor555) in saline with and without 0.042 mg/mL FITC-dextran (Molecular Probes, #D-7136, 500kD) were prepared. AlexaFluor555 particles were necessary, in place of Cy5.5, to match the optics of the available *in vivo* imaging system. SCION/FITC-dextran solutions were used for injections in B6-albino mice and only SCION solution for CD11c-EYFP and *lys*-EGFP mice, while saline controls were given to both. A volume of 10 μL was intracutaneously injected into the hind footpads of each anesthesized mouse (2.5% isofluorane in an air/O_2 mix) and the lymphatics to the popliteal LN were surgically exposed and imaged with a Olympus OV100 *in vivo* fluorescence imaging system pre-/during, 15 min, 30 min post-, or 24 hr post-injection. After obtaining *in vivo* images, lymphadenectomy of the popliteal LN was performed and the tissues fixed overnight in medium containing 0.05 M phosphate buffer, 0.1 M L-lysine, pH 7.4, 2 mg/ml $NaIO_4$, and 10 mg/ml paraformaldehyde. This fixation was followed by dehydration in 30% sucrose in phosphate buffer. Tissues were frozen in Tissue-Tek OCT medium (Sakura Finetek) on dry ice. 12–16 μm frozen sections were cut on a LEICA CM 3050s cryostat and and adhered to Superfrost Plus slides (VWR). Sections were blocked in PBS containing 10% goat serum (Jackson Immuno-Research Laboratories) and stained with unconjugated rat anti-mouse CD169 (Cedarlane, CL89149B) and rabbit anti-LVYE1 (Novus Biologicals). This was followed by incubation with AlexaFluor647-conjugated goat anti-rat IgG (Molecular Probes) and AlexaFluor405-conjugated goat anti-rabbit IgG (Molecular Probes). Three-dimensional image stacks of tissue sections were acquired on an LSM 710 (Zeiss MicroImaging) confocal microscope. Separate images were collected for each fluorochrome and overlaid to obtain a multicolor image. The images were displayed as two-dimensional maximum intensity projections and analyzed using Zeiss LSM Image Browser software.

RESULTS

The particle synthesis process consistently and reproducibly generated SCION particles that remained stable even when stored for up to 12 months. The optically transparent silica shell maintained particle suspension stability by providing a strong negative surface charge (−45 to −50 mV), particularly in physiological pHs 6–9. The complete dual-imageable silica-coated iron oxide nanoparticle (SCION), as shown in Fig. 1, had a diameter of 18–20 nm and iron content of 4.46 mmol Fe/g SCION, as measured by DLS and IEP-OES.

Relaxivities, r_1 and r_2, were determined from the slopes of the plot of relaxation rates, $R_1=1/T_1$ and $R_2=1/T_2$,vs [Fe or Gd] (Fig. 2). Both T_2 agents, Feridex (r_1 = 3.36 $mM^{-1}s^{-1}$) and SCION (r_1 = 1.34 $mM^{-1}s^{-1}$), had lower r_1 than the standard T_1 (r_1 = 4.29 $mM^{-1}s^{-1}$) agent Gd- DTPA. Feridex and SCION had more than 16 times enhanced r_2, respectively 145.83 and 87.78 $mM^{-1}s^{-1}$, compared to Gd-DTPA's 5.27 $mM^{-1}s^{-1}$. SCION had a lower r_1 and r_2 than Feridex.

In vivo, the prescence of SCION(Cy5.5) was observed in the draining axillary lymph node, (*i.e.* "sentinel node"), through both magnetic resonance and fluorescence images as presented in Fig. 3. The white arrows point to control nodes on the side with saline injection and the red arrows point to the nodes that were lower in signal on MR or enhanced during optical imaging after SCION(Cy5.5) injection. In optical imaging, the lateral thoracic node, which drains near and from the axillary lymph node, was also enhanced. When harvested from the body, the nodes continued to fluoresce. Histology confirmed SCION presence by staining positive for iron in nodes that showed contrast on MR or NIR imaging. Control nodes displayed no iron staining. The samples demonstrate that the particle enters the lymph node from afferent lymphatic vessels to the subcapsular sinus (Fig. 4a–d) and into the cortical sinuses (Fig. 4e–f).

Though nodes were invisible to the naked eye, they had an intense NIR enhancement. Fig. 5 demonstrates the location of a sentinel node through the skin of the mouse. A limitation of the optical image, however, is that the margins of the node are difficult to discern due to light diffusion. The MR image has a much higher spatial resolution allowing for some nodal anatomy to be deciphered. Of note, while an injection of 10 μL of a 40 mM [Fe] solution was necessary to consistently identify the lymph nodes using a 3-Tesla MRI instrument, nodes were detectable by the more sensitive optical imaging with as little as 2 mM [Fe] SCION(Cy5.5) solution.

To understand the mechanism of agent transport from the intracutaneous injection site to LN, a second series of animal studies were conducted where the lymphatic vessel leading to the popliteal LN was exposed and imaged at timepoints from pre- to 24 h post-injections. Immediately after injection of SCION(AlexaFluor555) into the hind footpad, the lymphatic vessel was illuminated, indicating passive transport of the agent itself due to diffusion into the vessel and lymphatic pressure and flow (see Video 1). Active cell-mediated transport through uptake by tissue resident dendritic cells (DCs) was studied at 24 h post-injection. No co-localization was found of the SCION agent with CD11c+ DCs labeled with YFP (see Video 2). Punctate movement of SCION was observed, however not in concurrence with CD11c+ DCs. Yet the primary mechanism for LN uptake post-intradermal injection appeared to be by non-active drainage of the agent itself. Images of the hind footpad injection site at various time points post-injection show that the majority of the agent drained quickly and was almost completely gone by 24 h (Fig. 6).

Confocal microscopy of harvested popliteal LN tissue was then used to study the fate of the particles upon arrival into the lymph node. FITC-labeled dextran, that based on previous experience, is readily taken up by subcapsular macrophages was co-injected with SCION(AlexaFluor555) in B6 albino mice. As seen in Fig. 7a–e, the two agents had different localizations. While dextran was found in CD169+ subcapsular macrophages, SCION was distinctly not and rather was found in LYVE-1+ lymphatic endothelial cells lining the subcapsular floor. The particle also had minimal co-localization with *lys*+ myelomonoytic (Fig. 7h–i) and CD11c+ dendritic cells in the LN (Fig. 7f–g). The images correlated with the previous histology and Prussian-blue staining of the axillary LNs, in that the particle was found to be in the peripheral subcapsular space and enters through the trajectory travecula into the sinus regions around follicles to end up in the medulla. This

follows the natural lymph flow pattern with SCION particles reaching the efferent lymphatic region by 24 hr. At 30 min post-injection, although dextran had began to accumulate in CD169+ macrophages, SCION agent was not detected, even though intravital imaging indicated that the particle was flowing through the lymphatic vessels to the LN. Tissue dehydration and the fixation process may have removed either agent that did not accumulate in cells or did not aggregate.

DISCUSSION

Characterization of the synthesized SCIONs determined that they have the size (18–20 nm), surface charge (−45 to −50 mV), and optical and MR properties desirable for a nanoprobe to be used for *in vivo* applications. Their T_2 relaxation was 16 times that of the most commonly used clinical agent, Gd-DTPA. The relaxivity was lower than that of Feridex, and this reduction may be a result of particle size (Feridex = 80–150 nm)), ease of water exchange through coating pores, or differences in crystalline structure. It may be possible to enhance SCION relaxivity futher by doping the magnetite core with ions such as zinc [19] and manganese [20].

In vivo, SCION was observed in the sentinel axillary LNs by both MR and optical imaging within 24 hr post-injection. Thus, the combination of MR and optical imaging in one agent could potentially allow sentinel nodes to be examined and mapped by MRI prior to surgery, and then be detected intraoperatively to assist the surgeon, during surgical resection. Talanov and co-workers [21] employed a similar approach and shown dual-modality SLN imaging with a Cy5.5-Gd-PAMAM G6 dendrimer that was injected into the mammary fat pad of mice. While there is promise for dendrimer-based and other macromolecular agents use in MRL, USPIOs are the only agents that have been used clinically. Iron oxide agents have been shown to be the safest when compared to a number of nanoparticles [22] and *in vivo* toxicity data indicates no long-term implications when administered at clinically relevant concentrations [23]. Though *in vivo* toxicity of SCION has not yet been analyzed, previously conducted *in vitro* studies showed minimal effect on lymphocyte and monocyte viability after a clinically relevant incubation time [14].

Histology of the imaged LNs demonstrated the presence of SCION in the sinuses flanking fiberous trabeculae that stretched from the outer capsule into the cortex. Particles did not appear to be present in the follicles of the cortex where B cells typically reside and where germinal centers are formed due to lymphocyte activation. Though less densely packed to allow for lymph to flow, sinus spaces typically contain lymphocytes, reticular cells, and macrophages. Macrophages are known to have a propensity to take up iron particles [24] and DCs for uptake of large NPs [25,26] given their role as scavenger cells for the immune system. Thus, the two questions that arose at this point were 1) how did the particles migrate from injection site to the LN, and 2) in what type of LN cells, if any, do they localize?

Various nanomaterials (dendrimers, viral particles, liposomes, quantum dots, and various polymer-based nanoparticles) have been used to target LNs by intradermal injection [26–30], and movement of the agent from skin to primary draining LNs has been shown to occur through either cell-mediated uptake, typically by dendritic cells (DCs), or by drainage of the agent itself through afferent lymphatics. Macrophages in the skin are generally thought to be tissue-resident and non-migratory, whereas epidermal (Langerhans cells) and dermal DCs migrate to draining LN upon encounter with antigens and particulates [26]. DCs readily internalize a variety of particulate materials including apoptotic bodies, latex particles, liposomes, and polymer-based nanoparticles [25]. In fact, particulate antigens are more efficient than soluble antigens at inducing cytotoxic T lymphocyte responses once DCs that have captured them migrate to the LN to stimulate naive T cells [25]. Hence, induction of

antigen-specific immunity *in vivo* using nanoparticles as vaccine vehicles has become an active area of research [28], primarily with polymer and liposome-based particles [30]. Phagocytic monocytes also exit the bloodstream and take up microbial products in the skin, differentiate into DCs, and then migrate to the LNs [26].

To study the uptake mechanism of SCION particles, CD11c-EYFP mice were intracutaneously injected with SCION(AlexaFluor555) in the hind footpad. These transgenic mice have DCs, including the dermal and LN DCs of interest, that express enhanced yellow fluorescent protein. Observation of the lymphatic vessel during and post-injection revealed that the particle migrated from the injection site to the LN primarily passively by diffusion into lymphatic vessels and normal lymphatic flow. Minor secondary punctate migration was observed 24 hr post-injection, however the particle signal did not co-localize with CD11c+ DCs. These results are surprisingly different than what would have been expected, given the role and highly phagocytic nature of tissue resident DCs. The rapid decrease in SCION emissions at the footpad injection site further indicates direct drainage of the agent, as cell-mediated uptake typically occurs at later time points, i.e. 24 h post-injection, and for which one would expect to observe significant quantities of the agent remaining at the injection site. While small particles with diameters less than 40 nm have been shown to diffuse passively into lymphatic vessels [28], additional cell-mediated uptake by CD11c- cells was not expected. Though typically tissue-resident macrophages are thought not to migrate through lymphatics [26], there are studies which have questioned this assertion [31]. A few studies also suggest that neutrophils can capture particles in the periphery and transport them to LN [32]. Clearly, further studies must be conducted to determine what type of cell is facilitating active trafficking of SCION. The implication of the passive lymphatic uptake is that this agent can be applied for imaging of lymphatic flow and identifying SLNs, as well as to target LN-resident cell types.

But to understand the potential for targeting cells within the LN, it is first important to analyze the fate of untargeted SCION as it enters the LN. Quantum dots [27] and dextran-coated USPIOs [24] have been shown to be endocytosed by macrophages in the LN, whereas dendrimer-based agents tend to follow the pattern of lymph fluid, in through the afferent vessels and subcapuslar sinsus, and then out the efferent vessel [27]. Previous studies that analyzed LN uptake based on size found 20 nm particles to localize within LN-resident antigen-presenting cells (i.e. DCs, B cells, pDCs, and macrophages), as well as in the subcapsular, cortical and medullary sinuses [26].

LNs harvested from the three types of mice from various time points post-SCION injection were stained for LYVE-1 and CD169. LYVE-1 is a receptor for extracellular matrix glycosaminoglycan hyaluronan (HA) found on lymphatic vessel walls [33]. CD169 is a marker that identifies macrophage subpopulations, especially those that are metallophillic [34,35]. In the case of these lymph node tissues, CD169+ cells line the subcapsular space (SCS). While SCS macrophages are typically poorly phagocytoic [36], CD169+ cells have been observed to pick up particulate antigen and viral particles [35]. As was expected, FITC-labeled dextran was found in CD169+ cells, however, the same was not true for SCION. In fact, it was instead found in the LYVE-1+/CD169− endothelial cells lining the SCS floor. A large amount also accumulated in the hilum where there was high staining of LYVE-1. Viral particles have been similarly found in medullary LYVE-1+/CD169- lymphatic endothelial cells [35]. There was minimal overlap of particle with the CD11c+ DCs and *lys*+ myelomonoytic cells (macrophages and neutrophil granulocytes). Years of literature have repeatedly reported dextran-coated USPIOs are taken up by macrophages upon entering the LN; indeed, this phenomenon has even been envoked clinically [24]. The results here go to show the importance of surface funcationality, as SCION's silica shell is the primary difference in structure and it was not found in CD169+ SCS or *lys*+

macrophages. We theorize that SCION's silica functionalization is making it relatively more inert and allowing it to follow normal lymphatic flow patterns from the SCS, down sinuses flanking jutting trabeculae, into the medulla, through the hilum, and eventually out the efferent lymphatics (Fig. 8).

CONCLUSIONS

The synthesis and characterization of SCION is straightforward and reproducible where the optical dye can be interchanged with a fluorophore of desired wavelength. The iron oxide core has a strong T2 relaxivity that allows noninvasive imaging of anatomical structure by MRI. For *in vivo* application, a NIR dye such Cy5.5 can minimize absorption and autofluorescence by tissue to allow greater light penetration; e.g., this can assist the surgeon to locate SLN(s) intraoperatively [8,9]. Though in the case of a peritumoral injection it may be possible to have increased uptake by scavenger cells, the primary mechanism by which this agent appears to move through the lymphatic system both from injection site and in LN is by passive diffusion into lymphatic flow. Contrast-enhanced imaging offers the ability to diagnose lymphatic disease and dual-labeled agents that permit imaging with MRI and optical cameras are at the forefront of this science. In addition, agents such as SCION have the potential to incorporate or attach drugs to their structure, which may enable targeted therapy in conjunction with diagnostic imaging.

Supplementary Material

Refer to Web version on PubMed Central for supplementary material.

Acknowledgments

This research was supported by the Marshall Commission and the Intramural Research Program of the NIH, National Cancer Institute, Center for Cancer Research.

References

1. Morton D, Chan A. The concept of sentinel node localization: How it started. Seminars in Nucl Med. 2000; 30:4–10.
2. Bass SS, Cox CE, Ku NN, Berman C, Reintgen DS. The role of sentinel lymph node biopsy in breast cancer. J Am Coll Surg. 1999; 189:183–194. [PubMed: 10437841]
3. Scoggins CR, Chagpar AB, Martin RC, McMasters KM. Should sentinel lymph-node biopsy be used routinely for staging melanoma and breast cancers? Nature Clinical Practice Oncology. 2005; 2:448–455.
4. Leong SP. Selective sentinel lymphadenectomy for malignant melanoma. Surg Clin North Am. 2003; 83:157–185. [PubMed: 12691454]
5. Morita ET. Lymphoscintigraphy in the detection of sentinel lymph nodes. Cancer Treat Res. 2002; 111:9–37. [PubMed: 12380173]
6. Barrett T, Choyke PL, Kobayashi H. Imaging of the lymphatic system: New horizons. Contrast Media Mol Imaging. 2006; 1:230–245. [PubMed: 17191764]
7. Sharma R, Wendt JA, Rasmussen JC, et al. New horizons for imaging lymphatic function. Ann N Y Acad Sci. 2008; 1131:13–36. [PubMed: 18519956]
8. Grosenick D, Wabnitz H, Rinneberg H, Moestra KT, Schlag PM. Development of a time-domain optical mammograph and first in vivo applications. Appl Opt. 1999; 38:2927–2038. [PubMed: 18319875]
9. Weissleder R. A clearer vision for in vivo imaging. Nat Biotechnol. 2001; 19:316–317. [PubMed: 11283581]
10. Andersson-Engels S, Wilson BC. In vivo fluorescence in clinical oncology: Fundamental and practical issues. J Cell Pharmacol. 1992; 3:48–60.

11. Wagnières GA, Star WM, Wilson BC. In vivo fluorescence spectroscopy and imaging for oncological applications. Photochem Photobiol. 1998; 68:603–632. [PubMed: 9825692]
12. De Grand AM, Frangioni JV. An operational near-infrared fluorescence imaging system prototype for large animal surgery. Technol Cancer Res Treat. 2003; 2:553–62. [PubMed: 14640766]
13. Tanaka E, Choi HS, Fujii H, Bawendi MG, Frangioni JV. Image-guided oncologic surgery using invisible light: Completed pre-clinical development for sentinel lymph node mapping. Ann Surg Oncol. 2006; 13:1671–81. [PubMed: 17009138]
14. Bumb A, Regino CAS, Perkins MR, et al. Preparation and characterization of a magnetic and optical dual-modality molecular probe. Nanotechnology. 2010; 21:175704. [PubMed: 20368682]
15. Bumb A, Brechbiel MW, Choyke PL, et al. Synthesis and characterization of ultra-small superparamagnetic iron oxide nanoparticles thinly coated with silica. Nanotechnology. 2008; 19:335601. [PubMed: 19701448]
16. Kosaka N, Ogawa M, Sato N, Choyke PL, Kobayashi H. In vivo real-time, multicolor, quantum dot lymphatic imaging. J Invest Dermatol. 2009; 129:2818–2822. [PubMed: 19536144]
17. Lindquist RL, Shakhar G, Dudziak D, et al. Visualizing dendritic cell networks in vivo. Nat Immunol. 2004; 5:1243–1250. [PubMed: 15543150]
18. Faust N, Varas F, Kelly LM, Heck S, Graf T. Insertion of enhanced green fluorescent protein into the lysozyme gene creates mice with green fluorescent granulocytes and macrophages. Blood. 2000; 96:719–726. [PubMed: 10887140]
19. Bárcena C, Sraa AK, Chaubeyb GS, et al. Zinc ferrite nanoparticles as mri contrast agents. Chem Commun. 2008; 19:2224–2226.
20. Lee J-H, Huh Y-M, Jun Y-W, et al. Artificially engineered magnetic nanoparticles for ultra-sensitive molecular imaging. Nat Med. 2007; 13:95–99. [PubMed: 17187073]
21. Talanov VS, Regino CAS, Kobayashi H, et al. Dendrimer-based nanoprobe for dual modality magnetic resonance and fluorescence imaging. Nano Lett. 2006; 6:1459–1463. [PubMed: 16834429]
22. Gojova A, Guo B, Kota RS, et al. Induction of inflammation in vascular endothelial cells by metal oxide nanoparticles: Effect of particle composition. Environ Health Perspect. 2007; 115:403–409. [PubMed: 17431490]
23. Shubayev VI, Pisanic Ii TR, Jin S. Magnetic nanoparticles for theragnostics. Adv Drug Delivery Rev. 2009; 61:467–477.
24. Bellin MF, Roy C, Kinkel K, et al. Lymph node metastases: Safety and effectiveness of mr imaging with ultrasmall superparamagnetic iron oxide particles -initial clinical experience. Radiology. 1998; 207:799–808. [PubMed: 9609907]
25. Elamanchili P, Diwan M, Cao M, Samuel J. Characterization of poly(d,l-lactic-co-glycolic acid) based nanoparticulate system for enhanced delivery of antigens to dendritic cells. Vaccine. 2004; 22:2406–2412. [PubMed: 15193402]
26. Manolova V, Flace A, Bauer M, et al. Nanoparticles target distinct dendritic cell populations according to their size. Eur J Immunol. 2008; 38:1404–1413. [PubMed: 18389478]
27. Kobayashi H, Ogawa M, Kosaka N, Choyke PL, Urano Y. Multicolor imaging of lymphatic function with two nanomaterials: Quantum dot-labeled cancer cells and dendrimer-based optical agents. Nanomedicine. 2009; 4:411–419. [PubMed: 19505244]
28. Reddy ST, Swartz MA, Hubbell JA. Targeting dendritic cells with biomaterials: Developing the next generation of vaccines. Trends Immunol. 2006; 27:573–579. [PubMed: 17049307]
29. Kim S, Lim YT, Soltesz EG, et al. Near-infrared fluorescent type ii quantum dots for sentinel lymph node mapping. Nat Biotechnol. 2004; 22:93–97. [PubMed: 14661026]
30. Reddy ST, Rehor A, Schmoekel HG, Hubbell JA, Swartz MA. In vivo targeting of dendritic cells in lymph nodes with poly(propylene sulfide) nanoparticles. J Controlled Release. 2006; 112:26–34.
31. Kirby AC, Coles MC, Kaye PM. Alveolar macrophages transport pathogens to lung draining lymph nodes. J Immunol. 2009; 183:1983–1989. [PubMed: 19620319]
32. Abadie V, Badell E, Douillard P, et al. Neutrophils rapidly migrate via lymphatics after mycobacterium bovis bcg intradermal vaccination and shuttle live bacilli to the draining lymph nodes. Blood. 2005; 106:1843–1850. [PubMed: 15886329]

33. Ji R, Kurihara K, Kato S. Lymphatic vascular endothelial hyaluronan receptor (lyve)-1- and ccl21-positive lymphatic compartments in the diabetic thymus. Anat Sci Int. 2006; 81:201–209. [PubMed: 17176958]

34. Kraal G, Janse M. Marginal metallophilic cells of the mouse spleen identified by a monoclonal antibody. Immunology. 1986:58.

35. Junt T, Moseman EA, Iannacone M, et al. Subcapsular sinus macrophages in lymph nodes clear lymph-borne viruses and present them to antiviral b cells. Nature. 2007; 450:110–114. [PubMed: 17934446]

36. Phan TG, Grigorova I, Okada T, Cyster JG. Subcapsular encounter and complement-dependent transport of immune complexes by lymph node b cells. Nat Immunol. 2007; 8:992–1000. [PubMed: 17660822]

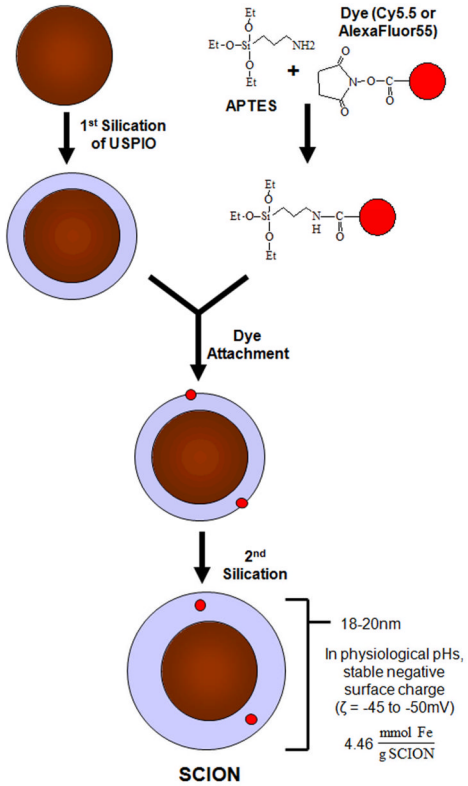

Fig. 1.
Synthesis of dual-modality silica-coated iron oxide nanoparticle (SCION)

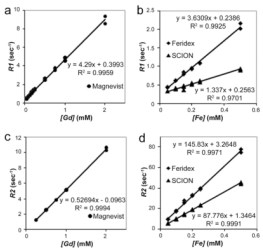

Fig. 2.

Relaxivity measurements ($mM^{-1}s^{-1}$) in a 3T magnet of SCION (r_1=1.34, r_2=87.78) compared to the larger iron oxide agent Feridex (r_1=3.63, r_2=145.83) and clinically used Gd-DTPA (Magnevist) (r_1= 4.29, r_2=5.27): (a) and (b) r_1 analysis and (c) and (d) r_2 analysis

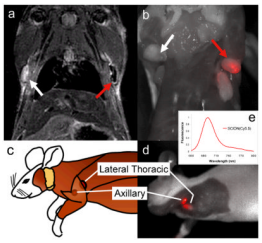

Fig. 3.

Sentinel lymph node imaging with SCION. The white arrows in (a) T_2-weighted MR and (b) optical imaging point to control nodes on which side a saline injection was given to the foot pad. The red arrows indicate nodes that were clearly visualized after SCION(Cy5.5) footpad injection, where in MR the node darkened and in spectrally unmixed optical imaging the NIR fluorescence was captured. The illuminated nodes are the axillary and lateral thoracic lymph nodes, as pointed out in (c) and (d). (e) The emissions spectrum of SCION(Cy5.5).

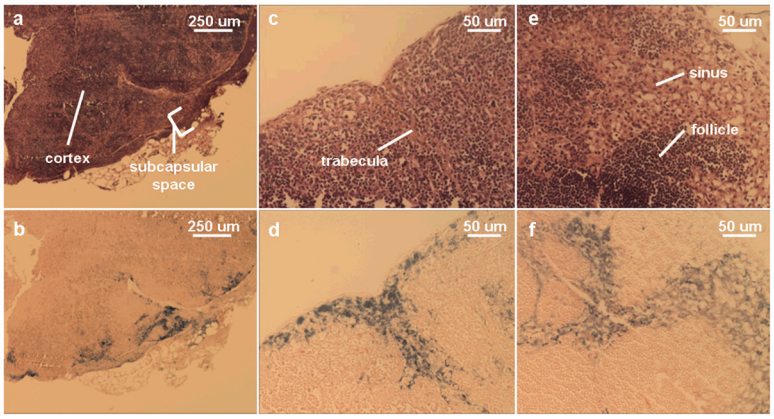

Fig. 4.

Matching H&E and Prussian blue iron staining of three nodes (a&b, c&d, e&f) confirming particle presence in axillary sentinel lymph node detected by SCION(Cy5.5). Particle was found to have entered through the subcapsular space (a&b) down trabeculae (c&d) and into the cortex (e&f) where again it is found in the sinus flanking follicle areas

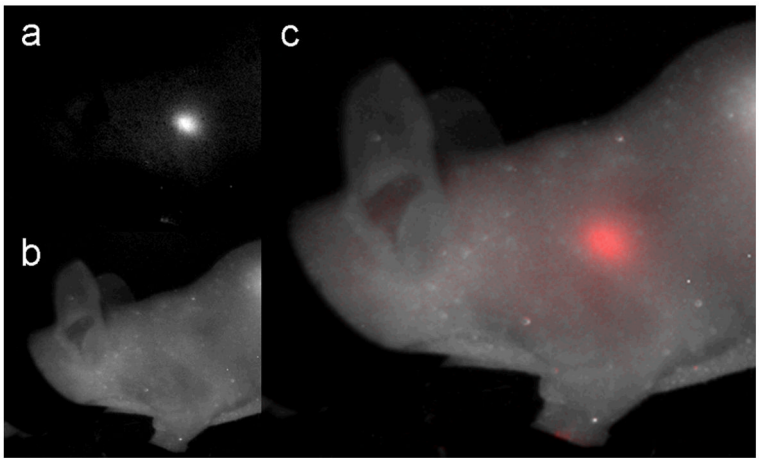

Fig. 5.

Spectral unmixing for optical imaging of sentinel lymph node with SCION(Cy5.5). The node is clearly visible through the skin in (c), the composite of (a) separated NIR light by SCION(Cy5.5) emissions (spectra Fig 3e) and (b) white light.

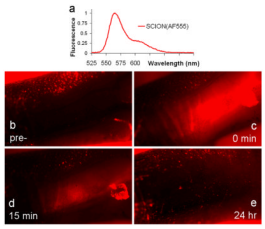

Fig. 6.

SCION(AlexaFluor555) emissions in hind footpad injection site (b) pre-, (c) immediately post-, (d) 15 min post-, and (e) 24 hr post-injection. The emissions spectrum of the injected agent is presented in (a). The red fluorescent signal seen in the pre-injection image and away from the injection site stemmed from autofluorescence, primary from hair follicles. Rapid clearance of particle from the intradermal injection site indicated that the primary mechanism of migration into lymphatics is passive diffusion

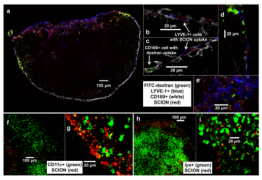

Fig. 7.

Confocal microscopy of SCION(AlexaFluor555) localization in politeal lymph node 24 hr post-intradermal injection in hind footpad. Panels b-e, g, and i are magnified regions of interest from LNs panels a, f, and h which capture the LNs as a whole or from their circumference. In all nodes, SCION was primarily found in the subcapsular space, trabelculae, and near the exiting efferent vessel in the medullary and hilum regions. (a-e) B6-albino mouse co-injected with FITC-dextran that localized in CD169+ subcapsular macrophages, whereas SCION particle was observed in LYVE-1+ endothelial cells lining the subcapsular floor (b-d) and hilum (a,e). (f-g) CD11c-EYFP mouse showed minimal uptake of SCION by CD11c+ dendritic cells. (h-i) *lys*-EGFP mouse biopsy found minimal overlap between SCION and *lys*+ myelomonocytic cells (neutrophil granulocytes and macrophages)

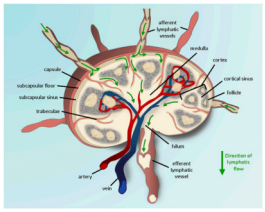

Fig. 8.
Flow of lymph fluid and SCION through lymph node